Confronting predictions of the galaxy stellar mass function with observations at high redshift

Article (Published Version)

Monthly Notices
of the
ROYAL ASTRONOMICAL SOCIETY

MNRAS **429,** 2098–2103 (2013) doi:10.1093/mnras/sts480

Confronting predictions of the galaxy stellar mass function with observations at high redshift

Stephen M. Wilkins,[1]⋆ Tiziana Di Matteo,[1,2] Rupert Croft,[1,2] Nishikanta Khandai,[2,3] Yu Feng,[2] Andrew Bunker[1] and William Coulton[1]

[1]*Department of Physics, University of Oxford, Denys Wilkinson Building, Keble Road, Oxford OX1 3RH*
[2]*McWilliams Center for Cosmology, Carnegie Mellon University, 5000 Forbes Avenue, Pittsburgh, PA 15213, USA*
[3]*Brookhaven National Laboratory, Department of Physics, Upton, NY 11973, USA*

Accepted 2012 November 22. Received 2012 November 22; in original form 2012 October 11

ABSTRACT

We investigate the evolution of the galaxy stellar mass function at high redshift ($z \geq 5$) using a pair of large cosmological hydrodynamical simulations: *MassiveBlack* and *MassiveBlack-II*. By combining these simulations, we can study the properties of galaxies with stellar masses greater than $10^8\,\mathrm{M}_\odot\,h^{-1}$ and (comoving) number densities of $\log_{10}(\phi\,[\mathrm{Mpc}^{-3}\,\mathrm{dex}^{-1}\,h^3]) > -8$. Observational determinations of the galaxy stellar mass function at very high redshift typically assume a relation between the observed ultraviolet (UV) luminosity and stellar mass-to-light ratio which is applied to high-redshift samples in order to estimate stellar masses. This relation can also be measured from the simulations. We do this, finding two significant differences with the usual observational assumption: it evolves strongly with redshift and has a different shape. Using this relation to make a consistent comparison between galaxy stellar mass functions, we find that at $z = 6$ and above the simulation predictions are in good agreement with observed data over the whole mass range. Without using the correct UV luminosity and stellar mass-to-light ratio, the discrepancy would be up to two orders of magnitude for large galaxies ($>10^{10}\,\mathrm{M}_\odot\,h^{-1}$). At $z = 5$, however, the stellar mass function for low-mass galaxies ($<10^9\,\mathrm{M}_\odot\,h^{-1}$) is overpredicted by factors of a few, consistent with the behaviour of the UV luminosity function, and perhaps a sign that feedback in the simulation is not efficient enough for these galaxies.

Key words: galaxies: high-redshift – galaxies: luminosity function, mass function – galaxies: stellar content.

1 INTRODUCTION

The observational exploration of the high-redshift ($z > 2$) Universe has been driven, over the past 10–15 years, predominantly by deep *Hubble Space Telescope* (*HST*) surveys. Deep Advanced Camera for Surveys (ACS) observations *alone* (e.g. of the Hubble Ultra Deep Field [HUDF]) permitted the identification of a large number of galaxies at $z = 2$–6 (e.g. Bunker et al. 2004; Beckwith et al. 2006; Bouwens et al. 2007). While some galaxies at $z > 7$ were identified using ACS and near-infrared (near-IR) Camera and Multi-Object Spectrometer (NICMOS) observations (e.g. Bouwens et al. 2008) or ground-based imaging (e.g. Bouwens et al. 2008; Ouchi et al. 2009; Hickey et al. 2010), the very high redshift Universe was only truly opened up by the installation of Wide Field Camera 3 (WFC3) in 2009. WFC3 near-IR (1.0–1.6 μm) observations allow the identification of star-forming galaxies to $z = 7$–8 (e.g. Bouwens et al. 2010, 2011b; Bunker et al. 2010; Oesch et al. 2010; Wilkins et al. 2010, 2011a; Lorenzoni et al. 2011) and potentially even to $z \sim 10$ (Bouwens et al. 2011a; Oesch et al. 2012).

By combining ACS optical and NICMOS or WFC3 near-IR imaging with *Spitzer* Infrared Array Camera (IRAC) observations, it becomes possible to probe the rest-frame ultraviolet–optical (UV–optical) spectral energy distributions (SEDs) of galaxies at $z = 4-8$ (e.g. Eyles et al. 2005; Gonzalez et al. 2012). Rest-frame optical photometry is crucial to accurately determine stellar masses (e.g. Eyles et al. 2007; Stark et al. 2009; Labbé et al. 2010; González et al. 2011, 2012). With a sufficiently large, well-defined sample of galaxies it is possible to study the galaxy stellar mass demographics, and in particular the galaxy stellar mass function (GSMF; e.g. González et al. 2011, 2012). The GSMF is a fundamental description of the galaxy population and is defined as the number density of galaxies per logarithmic stellar mass bin. The first moment of the GSMF corresponds to the cosmic stellar mass density.

⋆ E-mail: stephen.wilkins@physics.ox.ac.uk

Here we use state-of-the-art cosmological hydrodynamical simulations of structure formation (*MassiveBlack* and *MassiveBlack-II*) to investigate their predictions of the GSMF and compare it with current constraints. These runs are large, high-resolution simulations, with more than 65.5 billion resolution elements used in a box of roughly cubic gigaparsec scales (for *MassiveBlack*), making it by far the largest cosmological smooth particle hydrodynamics (SPH) simulation to date with 'full physics' of galaxy formation (meaning here an inclusion of radiative cooling, star formation, black hole growth and associated feedback physics) ever carried out. The combination of the two simulations allows us to probe galaxies with stellar masses greater than $10^8\,\mathrm{M}_\odot\,h^{-1}$ and (comoving) number densities of $\log_{10}(\phi[\mathrm{Mpc}^{-3}\,\mathrm{dex}^{-1}\,h^3]) > -8$, a range well matched with current observations at high redshift.

This paper is organized as follows. In Section 2, we introduce the *MassiveBlack* and *MassiveBlack-II* simulations. In Section 3, we explore the predicted evolution of the GSMF, how both the *intrinsic* and *observed* luminosities correlate with the stellar mass-to-light ratio, and in Section 3.5 compare GSMFs to recent observations. Finally, in Section 4 we present our conclusions.

Throughout this work, magnitudes are calculated using the AB system (Oke & Gunn 1983). We assume Salpeter (1955) stellar initial mass function (IMF), i.e. $\xi(m) = \mathrm{d}N/\mathrm{d}m \propto m^{-2.35}$.

2 *MassiveBlack* AND *MassiveBlack-II*

2.1 Simulation runs: *MassiveBlack* and *MassiveBlack-II*

Our new simulations (see Table 1 for the parameters of the simulation) have been performed with the cosmological TreePM-SPH code P-GADGET, a *hybrid* version of the parallel code GADGET2 (Springel 2005) which has been extensively modified and upgraded to run on the new generation of Petaflop-scale supercomputers (e.g. machines like the upcoming BlueWaters at NCSA). The major improvement over previous versions of GADGET is in the use of threads in both the gravity and SPH part of the code which allows the effective use of multi-core processors combined with an optimum number of MPI task per node. The *MassiveBlack* simulation contains $N_{\mathrm{part}} = 2 \times 3200^3 = 65.5$ billion particles in a volume of $533\,\mathrm{Mpc}\,h^{-1}$ on a side with a gravitational smoothing length $\epsilon = 5.0\,\mathrm{kpc}\,h^{-1}$ in comoving units. The gas and dark matter particle masses are $m_{\mathrm{g}} = 5.7 \times 10^7\,\mathrm{M}_\odot$ and $m_{\mathrm{DM}} = 2.8 \times 10^8\,\mathrm{M}_\odot$, respectively. The simulation has currently been run from $z = 159$ to 4.75 (beyond our original target redshift of $z = 6$). For this massive calculation, it is currently prohibitive to push it to $z = 0$ as this would require an unreasonable amount of computational time on the world's current fastest supercomputers. The simulated redshift range probes early structure formation and the emergence of the first galaxies and quasars.

MassiveBlack-II (see Khandai et al., in preparation for an overview) is a smaller volume but the mass and spatial resolution are better than *MassiveBlack* by a factor of 25 and 2.7, respectively. The smaller volume means that a smaller part of the high-mass function can be sampled and that in the mass range where it overlaps with *MassiveBlack* it can be used to check for convergence as well as to extend our predictions towards the low-mass end. This is the largest volume ever run at this resolution with a final redshift of $z = 0$.

These runs contain gravity and hydrodynamics but also extra physics (subgrid modelling) for star formation (Springel & Hernquist 2003), black holes and associated feedback processes (Di Matteo et al. 2008, 2012). The cosmological parameters used were the amplitude of mass fluctuations $\sigma_8 = 0.8$, spectral index $n_{\mathrm{s}} = 0.96$, cosmological constant parameter $\Omega_\Lambda = 0.74$, mass density parameter $\Omega_{\mathrm{m}} = 0.26$, baryon density parameter $\Omega_{\mathrm{b}} = 0.044$ and $h = 0.72$ (Hubble's constant in units of $100\,\mathrm{km\,s^{-1}\,Mpc^{-1}}$; *WMAP*5) for *MassiveBlack*. For *MassiveBlack-II* we instead used $\Omega_\Lambda = 0.725$ and $\Omega_{\mathrm{m}} = 0.275$ (according to *WMAP*7).

Catalogues of galaxies are made from the simulation outputs by first using a friends-of-friends groupfinder and then applying the SUBFIND algorithm (Springel 2001) to find gravitationally bound subhaloes. The stellar component of each subhalo consists of a number of star particles, each labelled with a mass and the redshift at which the star particle was created.

To generate the SED, and thus broad-band photometry, of each galaxy we sum the SEDs of each star particle (weighted by the particle mass). The SED of each star particle is generated using the PEGASE.2 stellar population synthesis (SPS) code (Fioc & Rocca-Volmerange 1997, 1999) taking their ages and metallicities into account. Nebula (continuum and line) emission is also added to each star particle SED, though this has a negligible effect on the UV photometry considered in this work. In addition, we apply a correction for absorption in the intergalactic medium using the standard Madau et al. (1996) prescription (though again this has a negligible effect on this work). Throughout this work, we measure the broad-band UV luminosity using an idealized rest-frame top-hat filter at $\lambda = 1500 \pm 200$ Å. A rest-frame filter is chosen to allow a consistent comparison between samples at different redshifts. The shape of this filter is selected for convenience, but closely reflects the profile of near-IR bandpasses which are available to measure the rest-frame UV flux at high redshift.

We note that our work is complementary to the recent simulation predictions of the GSMFs of Jaacks et al. (2012), who compare results for a suite of smaller simulations to the González et al. (2011, 2012) observational data. Our work differs in extending to a lower redshift, correcting for the effect of an evolving ratio of UV luminosity to mass-to-light ratio, and also for the inclusion of supermassive black hole formation and feedback in our simulations. We discuss the Jaacks et al. (2012) results further below.

Table 1. Main characteristics of *MassiveBlack* and *MassiveBlack-II* simulations. Both simulations included dark matter, SPH, a multi-phase model for star formation and a model for black hole accretion and feedback. N_{part} is the number of particles, L_{box} is the size of the simulation box, ϵ is the gravitational softening length, and z_{f} is the final redshift. Both runs were started at $z = 159$ and used six threads/MPI task. For *MassiveBlack-II*, the number of cores and threads used was optimized as it progressed.

Run	N_{part}	L_{box} ($\mathrm{Mpc}\,h^{-1}$)	ϵ ($\mathrm{kpc}\,h^{-1}$)	z_{f}
MassiveBlack	2×3200^3	533	5.0	4.75
MassiveBlack-II	2×1792^3	100	1.85	0

3 THE GALAXY STELLAR MASS FUNCTION

Measuring the GSMF from outputs of the *MassiveBlack* and *MassiveBlack-II* simulations is straightforward, given that the total masses of star particles in each galaxy are known. Before making a comparison to observational data, however, we must remember that observed UV luminosities were used (e.g. González et al. 2011, 2012) to compute the published observed GSMFs. This means examining the relationship between UV luminosity and stellar mass-to-light ratio in the simulation and using this information in our

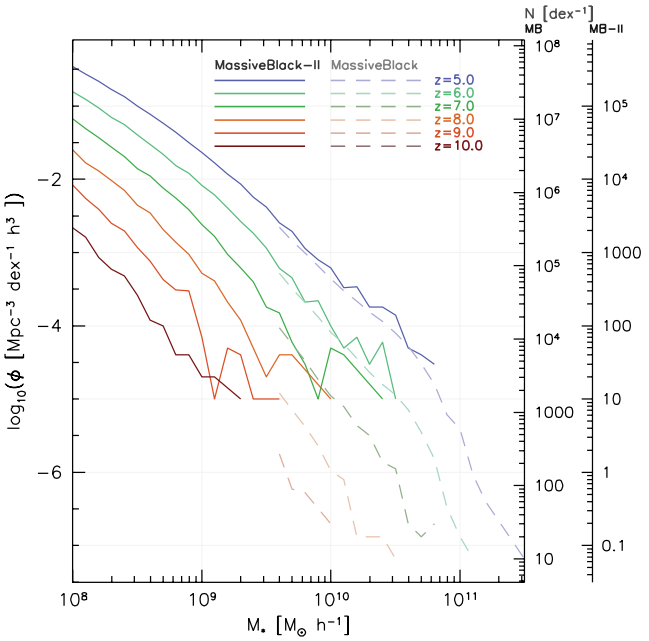

Figure 1. The GSMF measured from the *MassiveBlack* (dashed lines) and *MassiveBlack-II* (solid lines) simulations for $z \in \{5, 6, 7, 8, 9, 10\}$. The two right-hand axes show the number of galaxies in the *MassiveBlack* and *MassiveBlack-II* volumes.

comparison to observations. In this section, we do this after first presenting the GSMF measured directly from the simulations.

3.1 Galaxy stellar mass function from simulations

The evolution of the $>10^8$ M$_\odot$ h^{-1} GSMF from $z = 10$ to 5 predicted by *MassiveBlack* and *MassiveBlack-II* is shown in Fig. 1. The shape of the simulated GSMF is a declining distribution with mass and, at least at $z = 5$, exhibits a sharp cut-off at high masses. Values of the number density ϕ are also given in Table 2 in various logarithmic mass intervals.

Fig. 1 also demonstrates the evolution in the normalization of the GSMF. At $z = 10$ there are only ∼500 galaxies with stellar masses $>10^8$ M$_\odot$ h^{-1} in the *MassiveBlack-II* volume (10^6 Mpc^3 h^{-3}), while at $z = 5$ this has increased to ∼135 000 (×270). The shape of the GSMF also evolves strongly; while the number of galaxies with masses $>10^8$ M$_\odot$ h^{-1} increases by a factor of 270 from $z = 10$ to 5, the number of galaxies with masses $>10^{10}$ M$_\odot$ h^{-1} increases by a factor of 5000.

The evolution of the simulated GSMF is stronger than that exhibited by the UV luminosity function (LF). This reflects the fact that the average UV mass-to-light ratio of galaxies also increases $z = 10-5$ (as demonstrated in Section 3.3).

3.2 Observational estimation of the galaxy stellar mass function

By combining *HST* optical and near-IR observations (from ACS and NICMOS or WFC3) with *Spitzer* IRAC photometry, it is possible to measure the rest-frame UV–optical SEDs of high-redshift galaxies. Rest-frame optical photometry is vital to determine accurate stellar masses. Several studies have recently attempted to measure the stellar masses of high-redshift Lyman-break selected galaxies (e.g. Eyles et al. 2007; Stark et al. 2009; Labbé et al. 2010; González et al. 2011, 2012). With a sufficiently large sample and a handle on the incompleteness issues, it is also possible to study the GSMF (e.g. Stark et al. 2009; Labbé et al. 2010; González et al. 2011, 2012).

To understand how to make simulation predictions, it is useful to examine exactly how the González et al. (2011, 2012) GSMF is constructed. The González et al. (2011, 2012) study draws a sample of galaxies from the *observed* UV LFs at $z \in \{3.8, 5.0, 5.9, 6.8\}$ (using Bouwens et al. 2007, 2011b). These UV luminosities are converted into stellar masses using the *observed* UV luminosity ($L_{1500,\,\mathrm{obs}}$) versus stellar mass-to-light ratio (M/L$_{1500,\mathrm{obs}}$) distribution measured at $z \sim 4$. This relation is fairly well fit by a power law,[1] such that M/L$_{1500,\mathrm{obs}} \propto L^{0.7}$ (i.e. the stellar mass-to-light ratio increases with observed UV luminosity). While this relation is calibrated at $z = 4$, González et al. (2011, 2012) note that it appears to fit observations of stellar masses and luminosities at $z \in \{5, 5.9\}$. However, at these redshifts the sample sizes are small (78 and 28 galaxies at $z \sim 5$ and ∼6, respectively) and there is a large degree of scatter.

3.3 The relation between UV luminosity and the stellar mass-to-light ratio in simulations

As noted above, the González et al. (2011, 2012) study uses the distribution of stellar masses and UV luminosities measured at $z \sim 4$ to effectively convert the observed UV LF into a GSMF. To make a proper simulation prediction, we must take into account any difference between the relation between UV luminosity and the stellar mass-to-light ratio used by González et al. (2011, 2012) and that in the simulations.

Fig. 2 shows the relationship between the intrinsic UV luminosity (L_{1500}) and mass-to-light ratio (M/L$_{1500}$) at $z \in \{5, 6, 7, 8, 9, 10\}$ predicted by *MassiveBlack-II*. This relationship is (over the full mass range) approximately flat (i.e. the *intrinsic* stellar mass-to-light ratio is constant) and is significantly different from the M/L$_{1500,\mathrm{obs}} \propto L^{0.7}$ relation found by González et al. (2011, 2012). Jaacks et al. (2012) plotted the rest-frame UV magnitude against stellar mass in their simulations, also finding a flatter relationship than that used by González et al. (2011, 2012). The lower panel of Fig. 2 shows that the relationship between the intrinsic UV luminosity and stellar mass-to-light ratio also varies strongly with redshift, increasing by 0.6 dex from $z = 10$ to 5.

It is also interesting to note from Fig. 2 that it appears the *intrinsic* UV luminosity of galaxies with $L_{1500} > 10^{28}$ erg s^{-1} h^{-1} can *alone* be used to estimate the stellar mass with an accuracy of ≈50 per cent. This contrasts sharply with the low-redshift Universe where star formation has terminated in many systems (particularly massive ellipticals) rendering the UV luminosity to be negligible. The strong correlation between UV luminosity and stellar mass reflects the fact that virtually all galaxies at high redshift (in the *MassiveBlack* and *MassiveBlack-II* simulations) continue to actively form stars.

3.4 The effect of dust attenuation

The González et al. (2011, 2012) relation is however based on the *observed* (i.e. dust attenuated luminosities) as opposed to the *intrinsic* luminosities (as used in Fig. 2). Attenuation due to dust both decreases the UV luminosity (i.e. $L_{1500,\,\mathrm{obs}} < L_{1500}$) and *increases* the stellar mass-to-light ratio (i.e. M/L$_{1500,\mathrm{obs}}$ > M/L$_{1500}$) relative to their intrinsic values. A positive correlation between luminosity and dust attenuation would then introduce a positive correlation between M/L$_{1500,\mathrm{obs}}$ and the observed UV luminosity.

[1] Though the power-law fit is not used to determine the GSMF.

Table 2. The number density (in units of $\mathrm{Mpc}^{-3}\,\mathrm{dex}^{-1}\,h^3$) of galaxies in various logarithmic mass intervals ($[9.5, 10.0) \equiv 9.5 \leq \log_{10}(M) < 10.0$, where M has units $\mathrm{M}_\odot\,h^{-1}$) for $z \in \{5, 6, 7, 8, 9, 10\}$. Where there are no objects within the mass interval, the number density is replaced by an upper limit corresponding to $n < 1$ (i.e. $\phi < 1/V$).

Mass interval	$\log_{10}(\phi\,[\mathrm{Mpc}^{-3}\,\mathrm{dex}^{-1}\,h^3])$					
$\log_{10}([\mathrm{M}_\odot\,h^{-1}])$	$z=5$	$z=6$	$z=7$	$z=8$	$z=9$	$z=10$
	MassiveBlack Volume $= (533\,\mathrm{Mpc}\,h^{-1})^3$					
[9.5, 10.0)	−2.85	−3.50	−4.25	−5.13	−6.07	−7.88
[10.0, 10.5)	−3.69	−4.46	−5.35	−6.43	−7.88	<−8.18
[10.5, 11.0)	−4.55	−5.46	−6.80	−7.88	<−8.18	<−8.18
[11.0, 11.5)	−6.23	−7.88	<−8.18	<−8.18	<−8.18	<−8.18
[11.5, 12.0)	<−8.18	<−8.18	<−8.18	<−8.18	<−8.18	<−8.18
	MassiveBlack-II Volume $= (100\,\mathrm{Mpc}\,h^{-1})^3$					
[8.0, 8.5)	−0.70	−1.06	−1.46	−1.92	−2.44	−3.03
[8.5, 9.0)	−1.27	−1.69	−2.15	−2.69	−3.31	−4.06
[9.0, 9.5)	−1.95	−2.42	−3.01	−3.71	−4.47	−5.10
[9.5, 10.0)	−2.76	−3.37	−4.12	−4.80	−5.70	<−6.00
[10.0, 10.5)	−3.57	−4.27	−4.74	−5.70	<−6.00	<−6.00
[10.5, 11.0)	−4.40	<−6.00	<−6.00	<−6.00	<−6.00	<−6.00

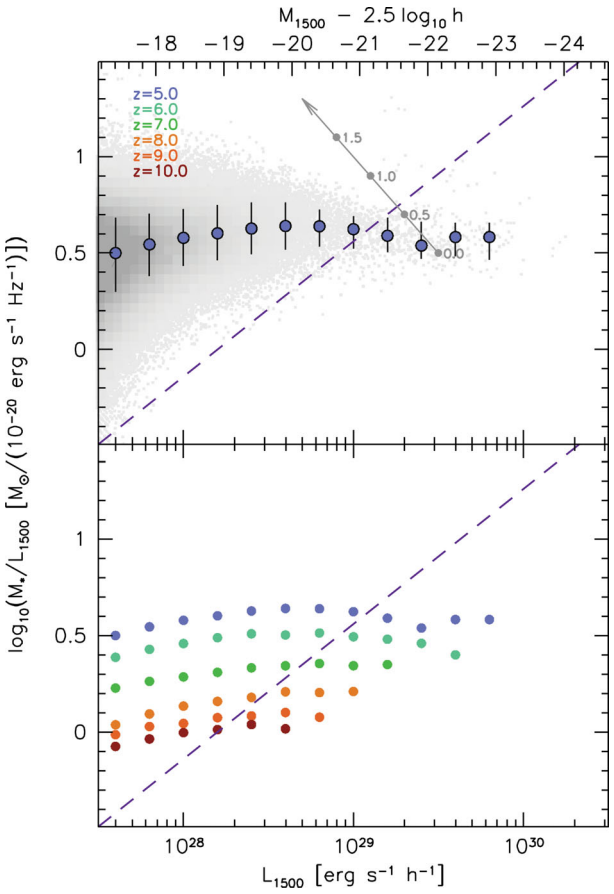

Figure 2. The relationship between the *intrinsic* UV luminosity and stellar mass-to-light ratio at $z \in \{5, 6, 7, 8, 9, 10\}$ predicted from *MassiveBlack-II*. In both panels, the points denote the median value of the mass-to-light ratio in each luminosity bin. In the upper panel, the 2D histogram shows the density of sources on a linear scale and the error bars show the range encompassing the central 68.2 per cent of the galaxies. The arrow in the upper panel shows the effect of dust attenuation (the labels denote values of A_{1500}). The dashed line in both panels shows $\mathrm{M/L}_{1500} \propto L^{0.7}$ which provides a good fit to the distribution used by González et al. (2011, 2012) to determine stellar masses from *observed* UV luminosities.

The measurement of dust attenuation at high redshift is challenging. Far-IR observations, and optical emission lines, are generally inaccessible for the bulk of the galaxy population at high redshift leaving only the UV continuum slope β as a diagnostic (e.g. Meurer et al. 1999; Wilkins et al. 2012a). A number of recent studies have attempted to constrain the relationship between β and the observed UV luminosity at high redshift though with some conflicting results (e.g. Stanway, McMahon & Bunker 2005; Bouwens et al. 2009, 2012; Wilkins et al. 2011b; Dunlop et al. 2012; Finkelstein et al. 2012). Bouwens et al. (2009), Wilkins et al. (2011b) and Bouwens et al. (2012) find an increase in β with observed luminosity. Dunlop et al. (2012) and Finkelstein et al. (2012), on the other hand, found little evidence of the variation of β with luminosity (see Wilkins et al., submitted for a detailed comparison).

Adopting the relationship(s)[2] between β and luminosity found by Bouwens et al. (2012) and utilizing the Meurer et al. (1999) calibration (between the observed UV continuum slope β and UV attenuation), we can determine the relationships between the observed UV luminosity ($L_{1500,\,\mathrm{obs}}$) and observed mass-to-light ratio at $z \in \{5, 6, 7\}$ as predicted by *MassiveBlack* and *MassiveBlack-II*. These are shown in Fig. 3. The most significant change (relative to that found for the intrinsic luminosities and mass-to-light ratios) is that the relationship between $L_{1500,\,\mathrm{obs}}$ and $\mathrm{M/L}_{1500,\mathrm{obs}}$ is no longer approximately constant but is instead strongly positively correlated, at least at $M_{1500,\,\mathrm{obs}} < -19.5$. At $M_{1500,\,\mathrm{obs}} < -19.5$ the slope of this relation is $\gamma = 0.5{-}0.8$ (where γ is defined such that $\mathrm{M/L}_{1500,\mathrm{obs}} \propto L^{\gamma}$) (cf. $\gamma = 0.7$ found by González et al. 2011, 2012 at $z = 4$). This suggests that the physical cause of the strong observed correlation between UV luminosity and mass-to-light ratio is caused almost solely by the correlation of dust attenuation with luminosity. At lower luminosities the relation flattens ($\gamma < 0.2$). This arises due to the diminishing effect of dust at lower luminosities, i.e. the $L_{1500,\,\mathrm{obs}}$–$\mathrm{M/L}_{1500,\mathrm{obs}}$ begins to reflect the (virtually flat) intrinsic relation.

[2] If a luminosity-invariant dust correction was assumed, the shape of the observed UV luminosity–mass-to-light ratio relation would remain the same (though the average observed mass-to-light ratio would increase).

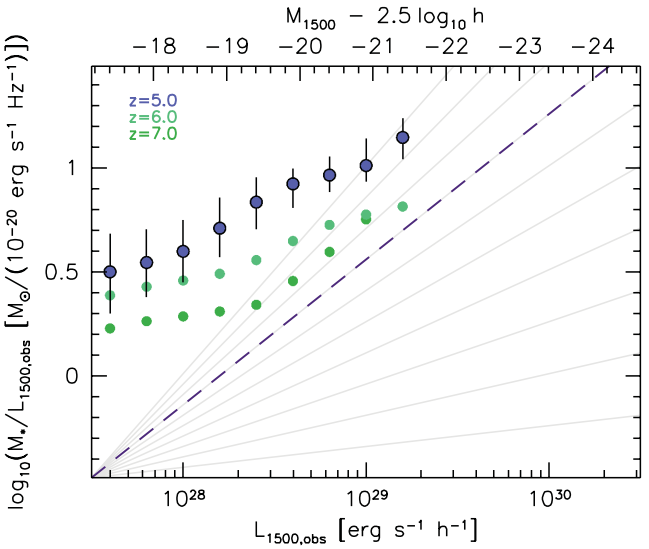

Figure 3. The relationship between the dust attenuated (observed) UV luminosity and stellar mass-to-light ratio at $z \in \{5, 6, 7\}$ predicted from *MassiveBlack-II* and using Bouwens et al. (2012) to relate dust attenuation to the observed UV luminosity. The points denote the median value of the mass-to-light ratio in each bin, while the vertical error bars (at $z = 5$) denote the 68.2 per cent confidence interval. The diagonal lines denote $M/L_{1500,obs} \propto L^{\gamma}$ for $\gamma = \{0.1, 0.2, \ldots, 1.0\}$. The dashed line denotes $\gamma = 0.7$.

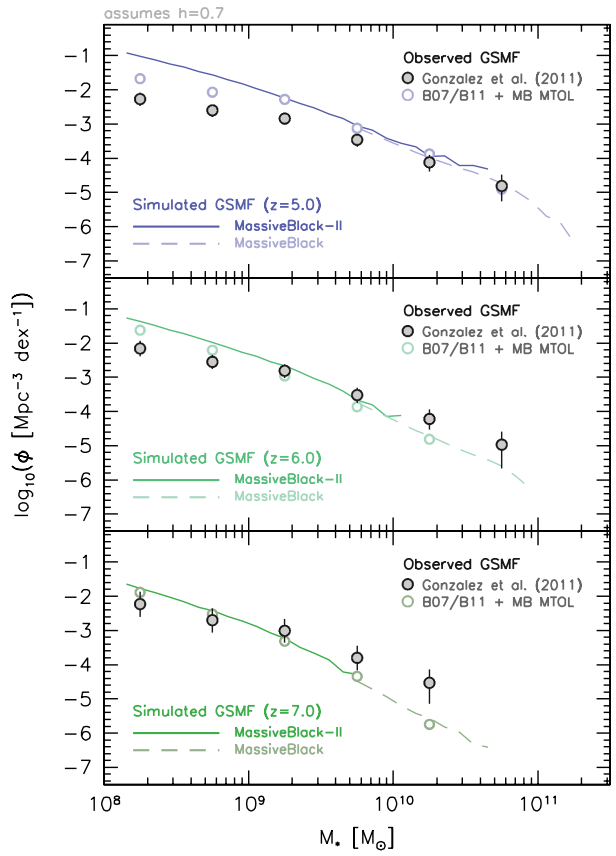

Figure 4. The GSMF predicted by *MassiveBlack* (dashed lines) and *MassiveBlack-II* (solid lines) compared with observations at $z \in \{5, 6, 7\}$ (top, middle and bottom panels, respectively). The open symbols in each panel show the prediction for the GSMF using the Bouwens et al. (2007, 2011b) observed UV LF and a relationship between stellar mass and luminosity derived from *MassiveBlack-II*. The filled grey points show the GSMF from González et al. (2011, 2012), which was estimated using a non-evolving relationship between UV luminosities and stellar mass-to-light ratios. Note that the units now implicitly assume $h = 0.7$.

3.5 Comparison with observations

We are now in position to compare the *MassiveBlack* and *MassiveBlack-II* results to observations. We follow a procedure similar to that of González et al. (2011, 2012) but using the simulated relation between UV luminosity and mass-to-light ratio. We construct a volume-limited sample (referred to below as 'B07/B11+MB MTOL') of galaxy UV luminosities using the Bouwens et al. (2007, 2011b) observed UV LFs. We then convert the *observed* UV luminosity of each galaxy to a stellar mass using the relation between luminosity and stellar mass-to-light ratio ($M/L_{1500,obs}$) predicted by the *MassiveBlack-II* simulation (combined with the empirical dust correction described above) and construct a GSMF. These GSMFs are shown at $z \in \{5, 6, 7\}$ in Fig. 4. We also show in Fig. 4 the GSMFs predicted by *MassiveBlack*/*MassiveBlack-II* and those determined by González et al. (2011, 2012) at $z \in \{5, 6, 7\}$ (the $z \sim 7$ GSMF comes from Labbé et al. 2010 but is also presented in González et al. 2011, 2012).

From an examination of Fig. 4, it is clear that the B07/B11+MB MTOL sample shows a much closer correspondence to the simulations as compared to that of González et al. (2011, 2012). This essentially reflects the good overall agreement between the simulated UV LF and the observations, at least at high luminosities. The flattening of the relation between $L_{1500,\,obs}$ and the mass-to-light ratio at low luminosities does go some way to explaining the difference in the shape of the simulated and observed GSMFs. More importantly however is the strong redshift evolution: from $z = 5$ to 7 the calibration relating the observed UV luminosity to the mass-to-light ratio decreases by 0.3–0.5 dex (depending on the luminosity). Because the González et al. (2011, 2012) study assumed no redshift evolution (instead utilizing a calibration based on observations at $z \sim 4$ to convert UV luminosities to stellar masses at $z = 4-7$), this would cause the stellar masses to be overestimated. Because the GSMF declines to high masses, this would cause the number density of sources at any mass to be overestimated.

We also note from Fig. 4 that at $z = 5$ (and to a lesser extent at $z = 6$) this process does not fully reconcile the GSMF at low masses. At $z = 5$, *MassiveBlack-II* overpredicts the faint end of the UV LF relative to the observations of Bouwens et al. (2007) by around a factor of 5 at $M_{1500} = -18$. This is difficult to reconcile observationally without requiring the application of a much larger completeness correction. It therefore suggests that the discrepancy has its roots in the *MassiveBlack*/*MassiveBlack-II* modelling assumptions. This disagreement occurs in low-mass galaxies which are much less affected by active galactic nucleus (AGN) feedback and hence more sensitive to the details of the star formation model and stellar feedback. For example, our model does not include any treatment of the molecular gas component such as e.g. in Krumholz & Gnedin (2011) which would tend to suppress star formation rates in lower mass galaxies. However, recent simulations of isolated galaxies (e.g. Hopkins, Quataert & Murray 2012) have shown that, in the presence of feedback, restricting star formation to molecular gas or modifying the cooling function has very little effects on the

star formation rates. By contrast, changing feedback mechanism or associated efficiencies translates in large differences in final stellar mass densities. Based on these recent results (albeit on idealized simulations), we are prone to interpret our discrepancy at the low-mass end to details in the stellar feedback model (and in particular to its efficiency which may be too low).

Comparing to the simulation results of Jaacks et al. (2012) (which do not include AGN modelling), we see a similar disagreement with observations at low mass. At the high-mass end, we have shown that correcting for the evolution of the relationship between UV luminosity and mass-to-light ratio brings the observations and simulations into agreement, and this would also be likely to work for the Jaacks et al. results. Finally, it is also worth noting that the González et al. (2011, 2012) GSMF evolves only very mildly from $z = 5$ to 7. Indeed, the stellar mass density (which is the first moment of the GSMF) of galaxies with $>10^8\,M_\odot$ is virtually flat $z = 5$–7. This is surprising given that all the galaxies contributing to the GSMF at these redshifts/masses are likely actively forming stars (by virtue of being UV selected) and suggest either the high-redshift GSMF is overestimated or the lower redshift GSMF is underestimated.

4 CONCLUSIONS

We have investigated the high-redshift ($z = 5$–10) evolution of the GSMF using a pair of large cosmological hydrodynamic simulations *MassiveBlack* and *MassiveBlack-II*. Over the redshift range $z = 10$–5, we find both the normalization and shape of the GSMF evolve strongly with the number density of massive galaxies ($>10^8\,M_\odot$) increasing by a factor of around 300.

By combining *HST* optical and near-IR observations (from ACS, NICMOS and WFC3) with near-IR IRAC photometry from the *Spitzer Space Telescope*, it is possible to identify and measure the stellar masses of galaxies at very high redshift, and thus constrain the GSMF (e.g. González et al. 2011, 2012). While the simulated GSMF at $z = 5$ provides reasonable agreement with the González et al. (2011, 2012) observations at $>10^{9.5}\,M_\odot$, at low masses and at $z > 5$ there is a significant discrepancy. The disagreement at low masses at $z = 5$ is also reflected in the UV LF at low luminosities. However, at $z > 5$ the discrepancy appears to arise due to a difference in the assumed relationship between the observed UV luminosity and mass-to-light ratio. González et al. (2011, 2012) apply a relationship calibrated at $z \sim 4$; however, we find that the relation, while having a similar form (i.e. the mass-to-light ratio is positively correlated with the observed UV luminosity), evolves strongly with redshift. Applying a calibration based on the simulated distribution of UV luminosities and stellar masses to the observed UV LFs yields GSMFs which closely reflect those predicted by the simulations. This simply reflects the good agreement between the observed and simulated intrinsic UV LFs.

ACKNOWLEDGMENTS

We would like to thanks Joseph Caruana and the anonymous referee for useful discussions and suggestions. SMW and AB acknowledge support from the Science and Technology Facilities Council. RC thanks the Leverhulme Trust for their award of a Visiting Professorship at the University of Oxford. WC acknowledges support from an Institute of Physics/Nuffield Foundation funded summer internship at the University of Oxford. The simulations were run on the Cray XT5 supercomputer Kraken at the National Institute for Computational Sciences. This research has been funded by the National Science Foundation (NSF) PetaApps program, OCI-0749212 and by NSF AST-1009781.

REFERENCES

Beckwith S. V. W. et al., 2006, AJ, 132, 1729
Bouwens R. J., Illingworth G. D., Franx M., Ford H., 2007, ApJ, 670, 928
Bouwens R. J., Illingworth G. D., Franx M., Ford H., 2008, ApJ, 686, 230
Bouwens R. J. et al., 2009, ApJ, 705, 936
Bouwens R. J. et al., 2010, ApJ, 709, 133
Bouwens R. J. et al., 2011a, Nat, 469, 504
Bouwens R. J. et al., 2011b, ApJ, 737, 90
Bouwens R. J. et al., 2012, ApJ, 754, 83
Bunker A. J., Stanway E. R., Ellis R. S., McMahon R. G., 2004, MNRAS, 355, 374
Bunker A. J. et al., 2010, MNRAS, 409, 855
Di Matteo T., Colberg J., Springel V., Hernquist L., Sijacki D., 2008, ApJ, 676, 33
Di Matteo T. et al., 2012, ApJ, 745, L29
Dunlop J. S., McLure R. J., Robertson B. E., Ellis R. S., Stark D. P., Cirasuolo M., de Ravel L., 2012, MNRAS, 420, 9
Eyles L. P. et al., 2005, MNRAS, 364, 443
Eyles L. P. et al., 2007, MNRAS, 374, 910
Finkelstein S. et al., 2012, ApJ, 756, 164
Fioc M., Rocca-Volmerange B., 1997, A&A, 326, 950
Fioc M., Rocca-Volmerange B., 1999, preprint (arXiv:astro-ph/9912179)
González V. et al., 2011, ApJ, 735, L34
González V., Bowens R. J., Labbé I., Illingworth G., Oesch P., Franx M., Magee D., 2012, ApJ, 755, 148
Hickey S., Bunker A., Jarvis M. J., Chiu K., Bonfield D., 2010, MNRAS, 404, 212
Hopkins P. F., Quataert E., Murray N., 2012, MNRAS, 421, 3488
Jaacks J., Choi J.-H., Nagamine K., Thompson R., Varghese S., 2012, MNRAS, 420, 1606
Krumholz M. R., Gnedin N. Y., 2011, ApJ, 729, 36
Labbé I. et al., 2010, ApJ, 716, L103
Lorenzoni S., Bunker A. J., Wilkins S. M., Stanway E. R., Jarvis M. J., Caruana J., 2011, MNRAS, 414, 1455
Madau P. et al., 1996, MNRAS, 283, 1388
Meurer G., Heckman T., Calzeth D., 1999, ApJ, 521, 64
Oesch P. A. et al., 2010, ApJ, 709, 21
Oesch P. A. et al., 2012, ApJ, 745, 110
Oke J. B., Gunn J. E., 1983, ApJ, 266, 713
Ouchi M. et al., 2009, ApJ, 706, 1136
Salpeter E. E., 1955, ApJ, 121, 161
Springel V., 2005, MNRAS, 364, 1105
Springel V., Hernquist L., 2003, MNRAS, 339, 289
Springel V., White S., Torman G., Kauffmann G., 2001, MNRAS, 328, 726
Stanway E. R., McMahon R. G., Bunker A. J., 2005, MNRAS, 359, 1184
Stark D. P., Ellis R. S., Bunker A. J., Bundy K., Targett T., Benson A., Lacy M., 2009, ApJ, 697, 1493
Wilkins S. M., Bunker A. J., Ellis R. S., Stark D., Stanway E. R., Chiu K., Lorenzoni S., Jarvis M. J., 2010, MNRAS, 403, 938
Wilkins S. M., Bunker A. J., Lorenzoni S., Caruana J., 2011a, MNRAS, 411, 23
Wilkins S., González-Perez V., Lacey C., Baugh C. M., 2012, MNRAS, 424, 1522
Wilkins S. M., Bunker A. J., Stanway E., Lorenzoni S., Caruana J., 2011b, MNRAS, 417, 717

This paper has been typeset from a TEX/LATEX file prepared by the author.